ACS APPLIED MATERIALS & INTERFACES

Research Article

www.acsami.org

Toward High Performance Thermoset/Carbon Nanotube Sheet Nanocomposites via Resistive Heating Assisted Infiltration and Cure

Jae-Woo Kim,*[,†] Godfrey Sauti,[†] Emilie J. Siochi,*[,‡] Joseph G. Smith,[‡] Russell A. Wincheski,[§] Roberto J. Cano,[‡] John W. Connell,[‡] and Kristopher E. Wise[‡]

[†]National Institute of Aerospace, Hampton, Virginia 23666, United States

[‡]Advanced Materials and Processing Branch, [§]Nondestructive Evaluation Science Branch, NASA Langley Research Center, Hampton, Virginia 23681, United States

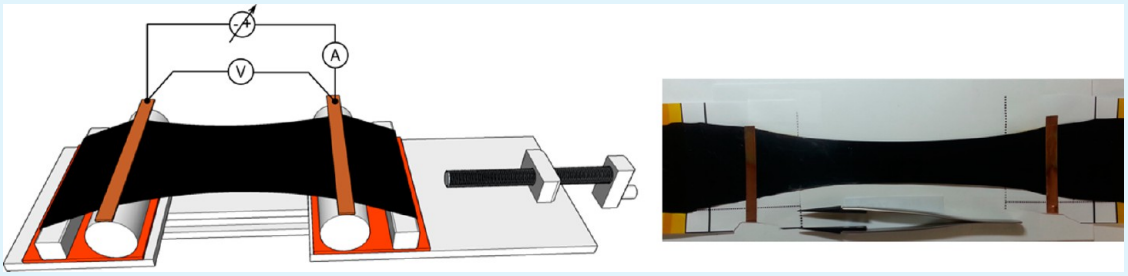

ABSTRACT: Thermoset/carbon nanotube (CNT) sheet nanocomposites were successfully fabricated by resistive heating assisted infiltration and cure (RHAIC) of the polymer matrix resin. Resistive heating takes advantage of the electrical and thermal conductivity of CNTs to rapidly and uniformly introduce heat into the CNT sheet. Heating the CNT sheet reduces the viscosity of the polymer resin due to localized temperature rise in close proximity to the resin, which enhances resin flow, penetration, and wetting of the CNT reinforcement. Once the resin infusion process is complete, the applied power is increased to raise the temperature of the CNT sheet, which rapidly cures the polymer matrix. Tensile tests were used to evaluate the mechanical properties of the processed thermoset/CNT sheet nanocomposites. The improved wetting and adhesion of the polymer resin to the CNT reinforcement yield significant improvement of thermoset/CNT nanocomposite mechanical properties. The highest specific tensile strength of bismaleimide(BMI)/CNT sheet nanocomposites was obtained to date was 684 MPa/(g/cm^3), using 4 V (2 A) for resin infiltration, followed by precure at 10 V (6 A) for 10 min and post curing at 240 °C for 6 h in an oven. The highest specific Young's modulus of BMI/CNT sheet nanocomposite was 71 GPa/(g/cm^3) using resistive heating infiltration at 8.3 V (4.7 A) for 3 min followed by resistive heating cure at 12.5 V (7 A) for 30 min. In both cases, the CNT sheets were stretched and held in tension to prevent relaxation of the aligned CNTs during the course of RHAIC.

KEYWORDS: *thermoset/carbon nanotube, nanocomposite, resistive heating*

1. INTRODUCTION

Carbon nanotubes (CNTs) are one-dimensional nanomaterials that have been touted for their outstanding combination of mechanical, electrical, and thermal properties. There is great interest in using them in lightweight structural applications because individual CNTs exhibit superior tensile elastic modulus (~1 TPa) and breaking strength (~100 GPa) on the nanoscale.[1−4] Although there has been some success in exploiting their electrical properties, the promising mechanical properties have not been retained in macroscale CNT nanocomposites fabricated using conventional methods.[5−9] This is primarily due to weak load transfer and interfacial interaction, both between tubes or tube bundles, and between the tubes and the polymer resin. Most studies on structural applications of CNTs have focused on attempts to improve CNT dispersion in engineering polymer matrixes to achieve enhanced mechanical properties of matrix resin in the resulting nanocomposites.[5−13] This approach to enhancing nanocomposite mechanical properties is limited by the small volume of CNTs that can practically be incorporated into the matrix without causing extremely high viscosities that impede processing of the nanocomposite precursor. Achieving nanocomposite mechanical properties that are competitive with state-of-the-art carbon fiber-reinforced polymer (CFRP) composites[14] requires higher loading levels, improved intertube and tube-resin load transfer, and the minimization of physical defect creation during processing and fabrication.

Although recent developments in high-volume manufacture of CNT sheets[15−17] and yarns[18−24] are improving the availability of these materials, infiltration of CNT assemblages such as yarns and sheets with high performance thermoset[25−29] and thermoplastic[30−32] polymers is quite challenging due to high resin viscosity, poor wettability, and low permeability of the CNT assemblages. These CNT forms exhibit small pore

Received: July 16, 2014
Accepted: October 3, 2014
Published: October 17, 2014

sizes (~10 nm)[33] and high resin flow path tortuosity, especially in highly densified formats. For example, the through-thickness permeability of CNT sheets to epoxy resin is very low (10^{-17}–10^{-19} m^2),[34] which results in void formation from trapped air in the processed materials, even when using enhanced processing techniques like vacuum assisted resin transfer molding (VARTM). Other processing techniques, such as in situ polymerization of polymer binders[35] and the direct application of a polymer resin during continuous drawing of aligned CNTs from spinnable CNT forests,[36−38] are being explored, but require further development.

Numerous methods of heating composites to promote polymer resin infusion and cure have been reported in the literature. Beyond conventional autoclave oven based approaches, microwave,[39,40] infrared,[41] ultrasonic,[42] inductive,[43] and electromechanical and electrothermal heating[44] methods have been used. The latter methods allow for targeted heating to specific zones, potentially minimizing the overall energy requirements. Because of the great difference in CNT and polymer thermal conductivities, heating tends to be greatest at this interface, which improves polymer mobility and accelerates cure. This has the beneficial effect of improving matrix/CNT interactions in that area, which is critical to nanocomposite mechanical properties. These techniques also allow for the fabrication of large structures because they operate outside the confines of conventional ovens. A related technique, resistive heating, has been developed as an approach for repairing localized damage in carbon fiber reinforced Surlyn ionomer[45] composites. Joule heating, resulting from the application of current to the carbon fibers, heats the ionomeric matrix to permit damage repair. Like carbon fiber, CNT sheets and yarns are excellent thermal and electrical conductors, making them amenable to resistive heating. In the present study, however, the heating is used for composite processing rather than damage repair.

In this work, high CNT content (>50 wt %) nanocomposites are fabricated from CNT sheet material using either SC-85 (a two-part epoxy system) or bismaleimide (BMI) for the matrix resin. A key step in this work is the introduction of resistive heating assisted infiltration and cure (RHAIC) to improve resin infiltration through the CNT sheet and to promote interfacial adhesion between the CNTs and the infiltrated resin to improve mechanical properties. RHAIC is a single, consolidated process that (1) integrates mechanical stretching of the CNT sheet to physically align CNTs, (2) efficiently infuses a minimum volume of resin to bond the aligned CNTs, (3) poststretches the predried "prepreg", and (4) cures the resin to complete fabrication of the CNT nanocomposite with optimal mechanical properties. The significance of this consolidated process is that all the necessary elements to fabricate and maximize the mechanical properties of CNT nanocomposites from CNT sheets are accomplished with a single, simple setup.

2. EXPERIMENTAL SECTION

2.1. Materials. The CNT starting materials used in this work were in the form of either an acetone treated CNT sheet [Lot# 5682-A (catalyst content, 10.8 wt %; average areal density, 10.00 g/m^2), Lot# 70044 (catalyst content, 10.4 wt %; average areal density, 11.61 g/m^2)] or a 0.3125 in. wide tape (Lot# 5166 thickness, 20 μm; catalyst content, 9.8 wt %; average areal density, 13.90 g/m^2) all purchased from Nanocomp Technologies, Inc. Thermosets used were SC-85 (two-part epoxy system, Applied Poleramic, Inc., USA, cure temperature, 38 °C for 2 h and 71 °C for 6 h postcure) and bismaleimide (BMI, RM-3010, Renegade Materials Corp., cured resin density, 1.25 g/cm^3; glass transition temperature, 279 °C (dry); resin flex strength, 124 MPa; resin flex modulus, 4.59 GPa; recommended cure condition, cure at 135 °C for 2 h, ramp to 182 °C, hold 6 h; postcure at 240 °C for 6 h). Toluene (Fisher Scientific, 99.9%) and methyl ethyl ketone (MEK, Sigma-Aldrich) were used as received.

Although the CNTs in the Nanocomp CNT sheet are largely randomly oriented, there is some directionality present as a result of the manufacturing process. All mechanical tests and stretching were conducted along this processing alignment direction. Generally, an as-received CNT sheet cut to 7 × 3 in. (17.78 × 7.62 cm) was used for fabrication of BMI/CNT sheet nanocomposites. The sheet was clamped on the custom built stretcher between two metal bars and then manually stretched to the desired level of stretching (from 0 to 48%) under ambient conditions. The level of stretching was calculated using length differences of marked lines [3 in. (7.62 cm) gap] at the center of the sheet before and after stretching.

2.2. Thermoset/CNT Sheet Nanocomposite Fabrication. Some of the CNT sheets used in this work were stretched with a custom-designed stretcher prior to the polymer infiltration step. The SC-85/CNT sheet nanocomposites were produced by painting the CNT sheet (pristine, acetone treated CNT sheet, or prestretched CNT sheets) with SC-85 (resin and hardener mixture) followed by RHAI. Increasing the applied current (or voltage) resulted in elevating the temperature to effect curing of the epoxy. The BMI/CNT sheet nanocomposites were fabricated by infiltration of the acetone treated (or its stretched) CNT sheet with a solution of BMI in toluene or MEK at various concentrations (0.01−2 wt %), followed by RHAIC. Accurate resistive heating was achieved at a very localized area by controlling voltage, current, and power with a suitable controller. Monitoring of the applied current and voltage was done using the Agilent E3632A (120W DC power supply) built-in current and voltage meters. To obtain detailed heating characteristics of the CNT sheet during processing, the E3632A power supply, Micro-Epsilon CT-SF22-C3 miniature infrared thermometers, and VIPER, a custom written LabVIEW based program were used to capture and record the voltage, current, and temperature. Temperature during processing of the material was also independently monitored using a Fluke VT02 Handheld Visual IR thermometer and Fluke 561 IR thermometer. The surface temperature of the CNT sheet was measured based on an emissivity of 0.76 obtained from a graphite surface.[46] The applied voltage changed the local temperature of the CNT sheet, which aided BMI infiltration through the CNT sheet and solvent evaporation, thus resulting in improved wettability and adhesion of the infiltrated BMI onto the CNT surfaces. Further increasing the applied voltage resulted in curing the BMI to lock in the aligned CNT networks. The infiltrated CNT sheets were cured using the following methods: conventional thermal method, RHAI followed by thermal cure, or RHAIC (resistive heating only, no additional thermal treatment). The thermal cure was conducted at 240 °C for 6 h in an air oven. RHAI consisted of two steps involving BMI infiltration at a lower applied voltage (3−5 V) for 3 min followed by precure at a higher applied voltage (10−15 V) for 5 min and then postcuring at 240 °C for 6 h. RHAIC was conducted at a higher applied voltage for a longer period of time (at least 30 min) to ensure that the cure process was complete.

2.3. Characterization. Room temperature tensile properties of the pristine CNT sheet, SC-85/CNT, and BMI/CNT nanocomposites were determined using a microtensile tester (Instron) or MTS-858 with a laser extensometer. An Instron 5848 microtester was used to measure force−displacement data of the pristine CNT sheets and lower strength materials. The specific elastic modulus, specific ultimate strength, and ultimate tensile strain were calculated subsequently. The MTS-858, equipped with a hydraulic grip and a laser extensometer, was used to test higher strength materials. This provided more accurate modulus data of the materials because errors associated with sample slippage in the grip were eliminated. Tensile stress was calculated by dividing the measured force by the cross-sectional area of the specimen. The thickness of films was determined with a profilometer-type instrument (Mitutoyo Corp., Model ID-S112PE) and confirmed by microscopic measurements. All mechanical data were normalized by the density of the specimen, which was

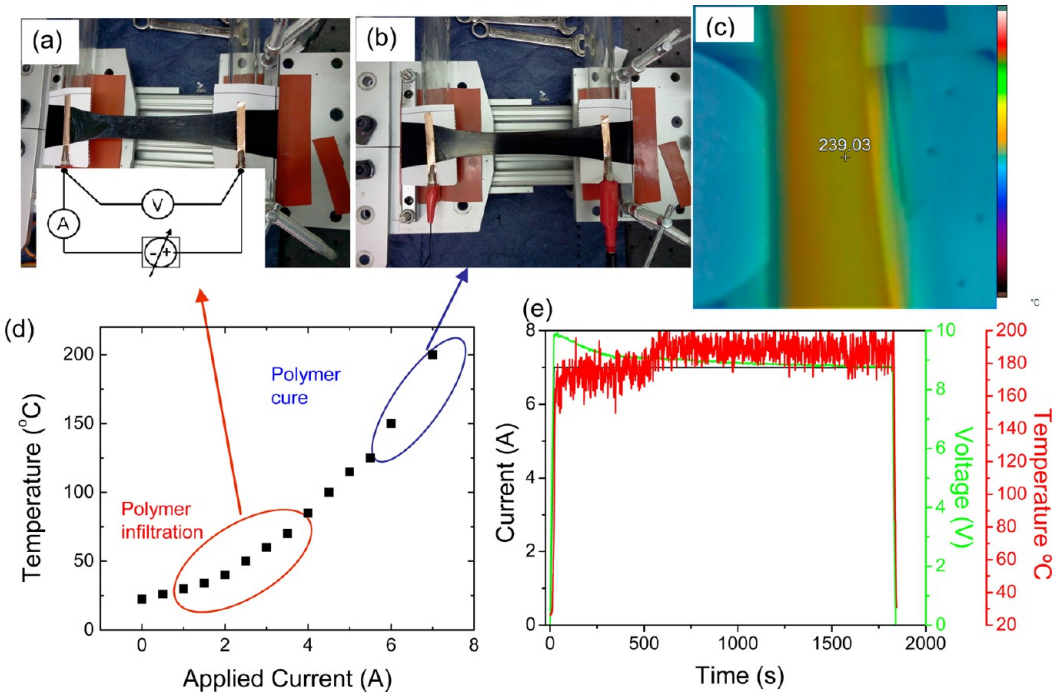

Figure 1. Pristine CNT sheet is loaded in a mechanical stretcher, stretched to the desired level, (a) infiltrated with resin, and (b) cured by resistive heating controlled by constant current or voltage. (c) 2-D infrared image with a representative temperature (°C) at a certain location during RHAIC. (d) Applied current vs temperature and (e) current−voltage−temperature vs time plot at constant current (7 A) with CNT sheet during BMI infiltration and curing by resistive heating.

determined by measuring the length, width, thickness, and weight of the specimen. The tensile testing methods were based on modified ASTM standards D882 (standard test method for tensile properties of thin plastic sheeting), D638 (standard test method for tensile properties of plastics), and D1708 (standard test method for tensile properties of plastics by use of microtensile specimens). The gage length was 10 mm for both the Instron (gap between the grips) and MTS-858 tensile tester (gap between two reflective tapes). The crosshead speed was 10 mm/min and 0.5 mm/min for pristine CNT sheets and polymer nanocomposites, respectively. The tensile samples were 5 mm wide rectangular strips. At least five specimens were tested to determine tensile strength and modulus. The Young's modulus was calculated by linear regression at the maximum slope for the data obtained from crosshead displacement and the slope between 10 and 30% of ultimate strength for the laser extensometer measurements. Toughness was calculated by measuring the area under the stress−strain curve up to material failure. The measured density of SC-85/CNT sheet nanocomposites was 0.983 ± 0.057 g/cm^3. The measured densities of BMI/CNT sheet nanocomposites ranged from 0.660 to 1.328 g/cm^3 depending on the level of stretching, polymer content, and processing history.

Field emission-scanning electron microscopy (FE-SEM, Hitachi Model S-5200) was used to image as-prepared polymer/CNT sheet nanocomposites and cross-sectional samples of failed specimens after tensile tests. A digital optical microscope (Mighty Scope) connected and controlled by Camtasia Studio 7 software (TechSmith Corporation) was used for monitoring in situ wetting and curing experiments of both SC-85 and BMI resin systems. Differential scanning calorimetry (DSC, Netzsch, Model DSC 204 F1) was carried out under nitrogen (20 mL/min) at heating rate of 10 °C/min. DSC thermographs were obtained by ramping to 350 °C followed by immediate quenching of the sample in liquid nitrogen. The same sample was then scanned again from room temperature to 400 °C. The chemical structure of the BMI/CNT sheet nanocomposites prepared by various cure conditions was studied using Fourier transform-infrared (FTIR, Thermo Nicolet, Model IR300 equipped with Thunderdome Swap-Top single reflection attenuated total reflectance module) spectroscopy. FTIR was carried out with as-prepared BMI/CNT sheet nanocomposites in the spectral range of 500−4000 cm^{-1}.

The two-dimensional (2-D) order parameter is equivalent to the Herman's orientation function for three-dimensional (3-D) systems and was determined by analysis of SEM images as follows: The edges of the aligned CNTs were detected as elliptical features by using the Canny edge detector in the Matlab GIAS-V2 tool. Around 1000 elliptical features were extracted from each SEM image to calculate the average angle. The average angle was based on an ellipse area weighted order, which was represented as a rose plot of the histogram of angular orientations. The 2-D order parameter ($S = 2\cos^2 \beta - 1$) of the aligned CNTs was calculated by using the average angles, β, between the local director and the main CNT aligned axis as described in ref 47.

3. RESULTS AND DISCUSSION

3.1. Concept of Resistive Heating Assisted Infiltration and Cure (RHAIC) for CNT Sheet Nanocomposite Process. The current approach to processing high performance nanocomposites using CNT sheets involves (1) mechanically stretching to align CNTs, (2) applying the matrix resin by painting, soaking, or spraying a resin solution, (3) predrying the coated sheet, (4) consolidating the predried sheets, and (5) finally completing the resin curing in a high temperature oven. With typical heating methods, this 5-step process requires two apparatuses−steps 1 through 3 can be carried out in a mechanical stretcher equipped with a sprayer, followed by steps 4 and 5, which require the coated sheet to be placed in an oven, for over 1 day for some material systems, to complete the cure. In RHAIC, all the necessary elements (stretching to align CNTs, applying the minimum amount of resin required to completely wet the CNTs, and curing of the polymer resin to lock in alignment of the CNTs for effective load carrying capability) are performed on a single device, as shown in Figures 1a,b. It is also notable that all of the materials

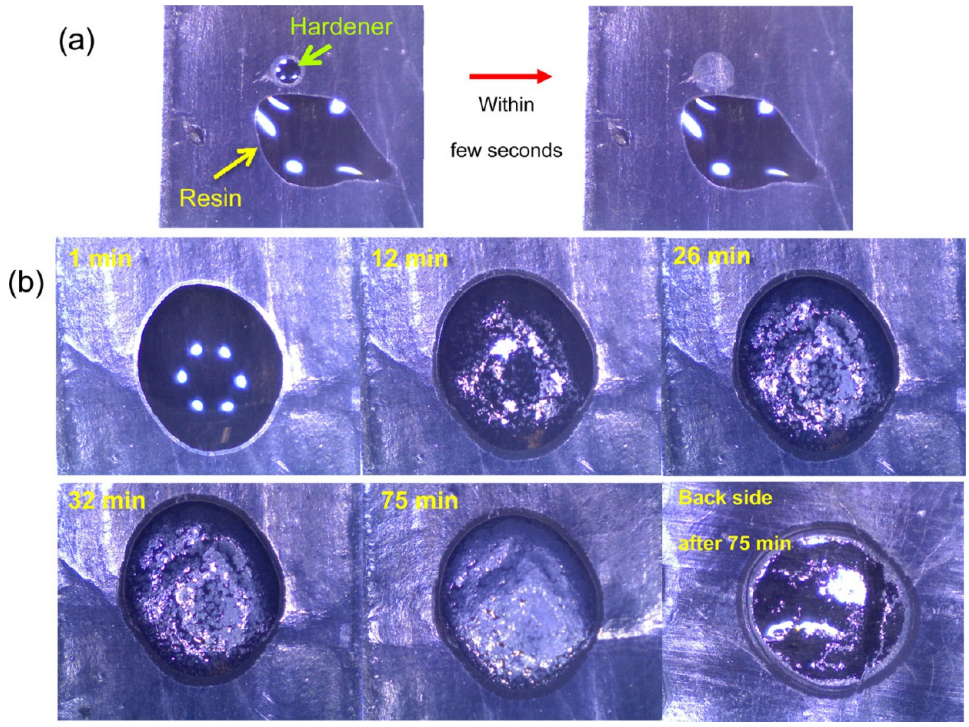

Figure 2. (a) Wetting study of SC-85 resin and hardener and (b) their mixture on pristine CNT tape without resistive heating.

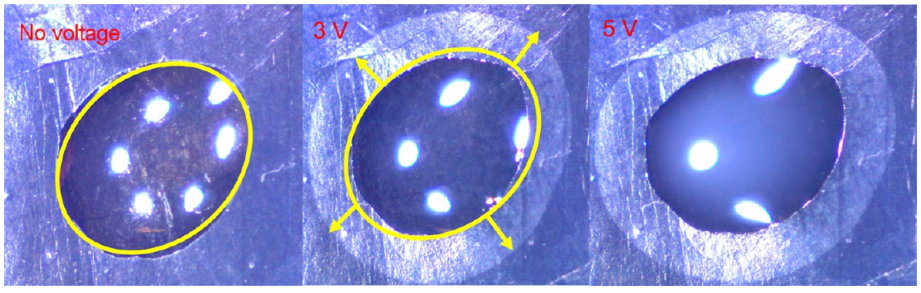

Figure 3. Wetting and curing study of a mixture of SC-85 resin and hardener on pristine CNT tape with resistive heating. The arrows represent the resin flow at 3 V.

processing steps can be completed within 1 h. The key difference is that the application of heat is done concurrently with the polymer addition, which allows steps 2–5 to be completed on the same setup. An additional oven-curing step is only required to ensure complete resin cure for high temperature polymers.

Figure 1c shows a two-dimensional (2-D) infrared (IR) image with a representative temperature at a stretched region of the CNT sheet during the RHAIC process. This image demonstrates the high degree of uniformity of temperature that is achieved using this technique. It should be noted, however, that maintaining a constant temperature during the cure process can be challenging due to changes in material emissivity and the emergence and movement of hot zones.

Figure 1d shows a representative current–temperature characteristic of a stretched (30%) CNT sheet with BMI resin (1 wt % BMI in toluene) over an infiltration and cure cycle. Varying the applied current allowed repeatable control of the sample temperature from room temperature to as high as 200 °C in air. The current–voltage–temperature versus time data is plotted during a cure cycle, as shown in Figure 1e. It can be seen that the desired temperature was achieved only a few seconds after the current was applied to the CNT sheet. Cooling also occurred rapidly after the applied current was turned off after the processing cycle was completed. Figure 1e shows that the temperature rapidly increased to 165 °C after a constant current (7 A) was applied to the sample. Heating of the CNT sheet resulted in decreased resistance, leading to a voltage drop across the sample. An apparent increase in temperature observed at ~600 s is most likely due to changes in the surface emissivity that resulted from the curing of the nanocomposites. The viscosity of applied resin was rapidly reduced at lower power (current × voltage) levels to enable complete wetting and infiltration of the CNT sheet with polymer resin (Figure 1a,d-marked) and removal of the solvent. In addition to the reduced resin viscosity at elevated temperatures, it is also possible that the interfacial tension changed, further aiding in resin flow and wetting.[48] Rapid resin curing is achieved by subsequently increasing the voltage (or current) to reach the recommended resin cure temperature (Figure 1b,d-marked). The resistive heating approach allows for a rapid increase in temperature and, due to the close spacing of the CNTs in the sheet, efficient and uniform thermal transfer to enable rapid curing of the matrix resin. Completing the cure

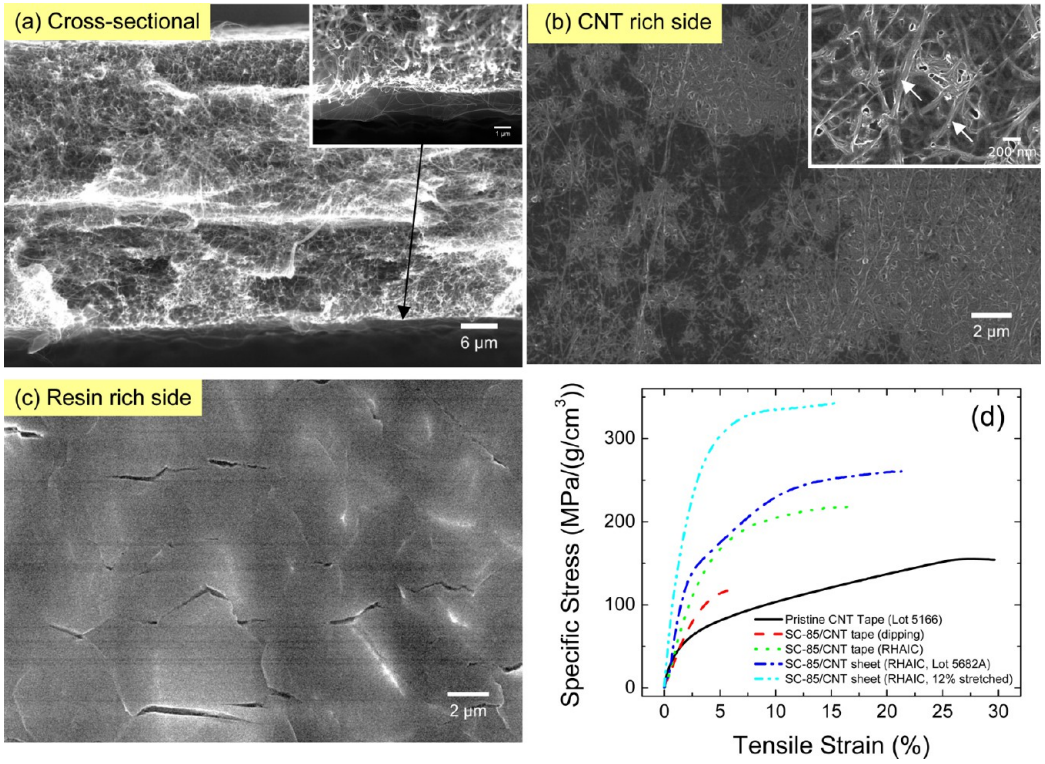

Figure 4. FE-SEM images of SC-85/CNT sheet nanocomposites: (a) cross-section after tensile failure, (b) CNT rich bottom, and (c) resin rich top surfaces. (d) Representative stress–strain curves of the processed SC-85/CNT sheet nanocomposites under a tensile load. The inset in panel a is a magnified cross-sectional image of the resin rich side. The inset in panel b is a magnified image of the CNT rich side. Arrows indicate CNT bundles with resin coating.

process while the nanocomposite is held in tension has the added advantage of locking in the alignment achieved by mechanical stretching of the CNT sheet. Removing the sample and placing it in an oven for cure, as required by the typical approach, allows for partial relaxation of the alignment achieved during stretching.

3.2. RHAIC–SC-85 Two-Part Resin System. For a detailed look at the wetting of the CNT sheet under resistive heating, a two-part epoxy resin system, SC-85, was used. All images in Figures 2 and 3 were collected in real time under an optical microscope. Figure 2a shows the result of depositing the SC-85 resin and hardener components separately on the CNT tape surface. While the low viscosity hardener quickly wetted the CNT tape, the more viscous resin did not fully wet and infiltrate the CNT tape. Figure 2b shows that mixing the resin and hardener prior to deposition still yielded viscosities that were too high to wet the CNT tape surface after application. The resin bead began to cure over time without significant penetration into the CNT tape and had almost completely hardened after 75 min. The hardener penetrated the CNT tape and accumulated on the backside (shiny residue on the backside surface in Figure 2b), suggesting that in the course of the experiment, the less viscous hardener phase separated from the resin due to mismatches in viscosity of the components and their differing chemical affinities for the CNTs.

In contrast to these results, Figure 3 shows that, when assisted by resistive heating, the SC-85 resin and hardener mixture wetted through the CNT tape uniformly. The series of images in Figure 3 indicates that the extent of infiltration and curing of SC-85 resin increased with increasing applied voltages, as reflected in the differences in transparency of the resin drops (clear to opaque). The lower applied voltage (3 V), center image in Figure 3, produced a temperature change in the CNT sheet sufficient to lower the viscosity of the resin mixture and promote uniform wetting within a few tens of seconds, but did not raise it enough to initiate curing. Further increasing the applied voltage to 5 V (Figure 3, right image) resulted in curing of the resin within a short period of time, as indicated by transparency change. In neither case was evidence of phase separated hardener residue observed on the backside of the CNT sheet.

On the basis of the results of the droplet experiments, SC-85/CNT sheet nanocomposite fabrication was performed by premixing the resin and hardener and using RHAIC to promote infiltration and cure. Morphologies of the fabricated SC-85/CNT sheet nanocomposites and their mechanical properties are summarized in Figure 4. Figure 4a shows that the SC-85/CNT sheet nanocomposites were well wetted and that interconnections between CNT bundles formed throughout the thickness of the film. Figures 4b and c, however, demonstrate that applying the resin to only one side resulted in CNT rich/resin poor (Figure 4b) and resin rich/CNT poor (Figure 4c) sides of the nanocomposite.

Despite this shortcoming, improvements in mechanical properties were significant (Figure 4d). The measured specific tensile strength and specific Young's modulus of the pristine CNT tape (Lot# 5166) were 156 ± 11 MPa/(g/cm^3) and 6.1 ± 1.5 GPa/(g/cm^3), respectively, and elongation at failure was 30 ± 8%. The mechanical properties of a dip coated and thermally cured SC-85/CNT nanocomposite were poor for both the specific tensile strength [119 MPa/(g/cm^3)] and specific modulus [3.4 GPa/(g/cm^3)] when the process was completed without RHAIC. Poor wetting (thick resin rich layer) and poor adhesion of the resin to the CNT tape were

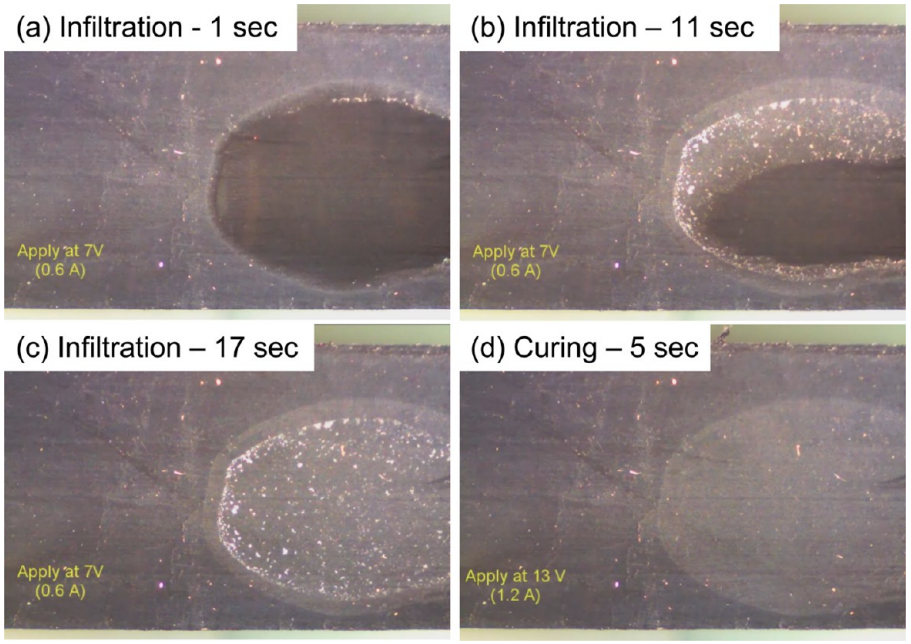

Figure 5. Wetting and curing study of BMI resin on the pristine CNT sheet with resistive heating. Optical microscopy images are captured at (a) 1, (b) 11, and (c) 17 s after applying a voltage of 7 V for infiltration and at (d) 5 s after applying a voltage of 13 V for cure.

Table 1. Physical and Mechanical Properties of Pristine and Processed BMI/CNT Sheet Nanocomposites[a]

sample	cure	BMI loading (wt %)	density (g/cm^3)	thickness (μm)	specific strength [$MPa/(g/cm^3)$]	specific modulus [$GPa/(g/cm^3)$]	elongation at failure (%)
1 pristine (Lot# 5682-A)		0	0.735	15.1	254 ± 13	6 ± 1	31 ± 2
2 BMI/CNT sheet[b]	thermal	33	0.756	23.5	357 ± 14	21 ± 2	16 ± 1
3 stretched CNT (S-CNT) sheet (33.9%)		0	0.882	15.7	367 ± 4	15 ± 0.1	7.3 ± 0.8
4 BMI/S-CNT sheet	thermal	24	0.867	20.0	412 ± 3	32 ± 4	2.6 ± 0.2
5 BMI/S-CNT sheet	thermal	43	1.144	21.0	541 ± 9	31 ± 3	3.9 ± 0.1
6 BMI/S-CNT sheet	RHAIC	18	0.836	21.3	461 ± 44	43 ± 3	5.1 ± 2.8
7 BMI/S-CNT sheet	RHAIC	39	1.172	19.1	609	71	3.0

[a]All BMI/S-CNT sheet nanocomposites were fabricated with a stretched (33.9%) CNT (S-CNT) sheet. [b]The BMI/CNT sheet nanocomposite was fabricated with Lot# 70044.

observed. In comparison, the specific tensile strength of SC-85/CNT nanocomposites fabricated from CNT tape by RHAIC was 218 $MPa/(g/cm^3)$. Employing acetone condensation to densify the CNT sheet prior to nanocomposite fabrication by RHAIC increased the specific strength to 284 $MPa/(g/cm^3)$. The specific strength was further increased to 347 $MPa/(g/cm^3)$ when the SC-85 resin was applied to acetone condensed and mechanically stretched CNT sheet. The Young's modulus of RHAIC processed SC-85/CNT sheet nanocomposites likewise increased to 10.1 and 14.5 $GPa/(g/cm^3)$ with unstretched acetone treated and stretched acetone treated CNT sheets, respectively. The specific tensile strength below 10% strain also dramatically increased due to better adhesion of the resin to the CNT surfaces. The SC-85/CNT sheet nanocomposites fabricated by RHAIC also exhibited improved toughnesses of 55 (unstretched) and 45 J/g (stretched) compared with samples produced by the dipping process followed by thermal cure with untreated CNT tape (5.3 J/g). Note that the toughness of untreated and acetone treated CNT sheets without resin were 35 and 51 J/g, respectively.

3.3. RHAIC–BMI One-Part Resin System. BMI, another thermoset system commonly used for engineering composites, was also investigated. BMI was dissolved in toluene or methyl ethyl ketone (MEK) to promote its ability to wet the CNT sheet. Solvents with proper boiling points and volatility, such as toluene (b.p.: 111 °C) and MEK (b.p.: 80 °C), have the advantage of keeping the CNT sheet wet during the resin infiltration step at lower applied voltage, and then quickly evaporating when the applied voltage is increased to initiate curing. The images in Figure 5 were taken with an optical microscope during infiltration and curing of a BMI/toluene solution into the CNT sheet. The infiltration phase of the RHAIC process (Figure 5a–c) was conducted at 7 V (0.6 A), followed by cure (Figure 5d) at 13 V (1.2 A). The BMI solution quickly wetted and infiltrated the CNT sheets within 20 s. The residual toluene evaporated within a few tens of seconds at the elevated temperature reached by resistive heating. Subsequently increasing the applied voltage to 13 V increased the local temperature of the CNT sheet to initiate cure of the resin (Figure 5d). Note that following this elevated temperature treatment, the BMI residue that was visible after solvent evaporation (white spots in Figure 5c) was no longer present. It should also be noted that the size of CNT sheet used for the wetting and curing test differs from that used in the actual nanocomposite fabrication. The size difference requires the use of different voltage–current settings to achieve a similar temperature response for the infiltration and cure steps.

A series of BMI/CNT sheet nanocomposites were prepared to study the effects of BMI loading levels, level of stretching, and cure conditions on their tensile properties (Table 1). Representative stress−strain curves of as-received and stretched CNT sheets, conventionally cured BMI/CNT sheet, and RHAIC-processed BMI/CNT sheet nanocomposites with different loading levels of BMI are shown in Figure 6. The

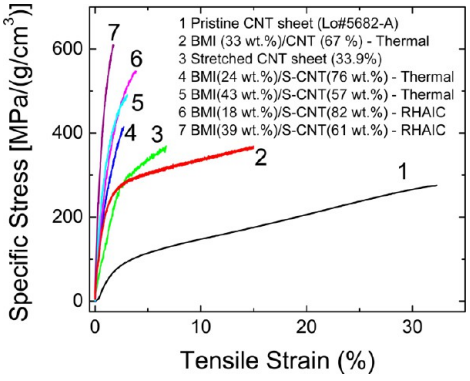

Figure 6. Representative stress−strain curves of the pristine CNT sheet and processed BMI/CNT sheet nanocomposites fabricated by thermal cure and RHAIC. All BMI/CNT sheet nanocomposites were fabricated with a stretched (33.9%) CNT (S-CNT) sheet.

effect of mechanically stretching the pristine sheet can be seen by comparing traces 1 and 3. Upon stretching by 33.9%, the specific strength increased from 254 to 367 MPa/(g/cm^3) and the specific Young's modulus increased from 5.9 to 14.5 GPa/(g/cm^3), which are in good agreement with the literature.[35,49] Further increases in tensile properties were achieved by BMI infiltration, both with lower (~20%, traces 4 and 6) and higher (~40%, traces 5 and 7) loading levels of BMI. This was observed in both thermally cured (traces 4 and 5) and RHAIC processed (traces 6 and 7) nanocomposites. In general, the specific strength and modulus of the BMI/CNT nanocomposites prepared by RHAIC were greater than those obtained from thermal curing when using similar degrees of BMI loading and CNT stretching. The greatest enhancement of mechanical properties was achieved with a BMI loading content of 39% using stretched CNT sheets as the reinforcement and the RHAIC method. To some extent, the improved mechanical properties observed in the RHAIC processed sheets arise from the fact that they are held in their stretched configuration while curing. The conventionally cured samples are, in contrast, removed from the stretching rig and placed in an oven to cure, which allows some degree of relaxation of the stretch-induced alignment of the CNTs in these samples. Being able to cure the sheets in their stretched configuration is one of the attractive features of the RHAIC method.

All of the specific strength and modulus data for the various processing treatments are plotted in Figures 7a,b, respectively. The mechanical properties are plotted as a function of the extent of stretching in an attempt to decouple the effects of stretching from the other processing variables. Increasing the alignment of the CNT bundles in the pristine sheets by stretching clearly resulted in moderate improvements in strength and modulus (black squares). Adding BMI to the stretched sheets without resistive heating, followed by thermal curing, resulted in substantial improvements in strength and smaller increases in modulus (pink triangles). Much larger increases in strength and modulus resulted from the use of resistive heating when adding the matrix polymer, regardless of whether thermal (blue triangles) or resistive heating (red circles) methods were used to cure the matrix. These improvements reflect the significantly improved infiltration and wetting that occurs when using RHAI. The data in Figure 7a indicate that the highest specific strength values were obtained by resistive heating followed by thermal curing in an oven. For specific modulus, on the other hand, the best results were achieved when the material was cured using resistive heating (Figure 7b). As mentioned above, this is not surprising because curing the material in the stretching rig prevents relaxation of CNT bundle alignment, which has a much larger impact on modulus than strength. The differences in specific strength and modulus observed between samples with similar levels of stretching resulted from different resin contents in the nanocomposites and the application of post stretching during the RHAIC process.

In view of the strong dependence of the measured mechanical properties on the extent of stretching, it is important to quantify the effect of stretching on CNT bundle orientation. The FE-SEM images shown in Figure 8 were used to calculate 2-D order parameters (S) for four representative samples produced in this study. Figure 8b,d shows high magnification images of the pristine CNT sheet before and after stretching by 31.2%. The visually obvious increase in alignment

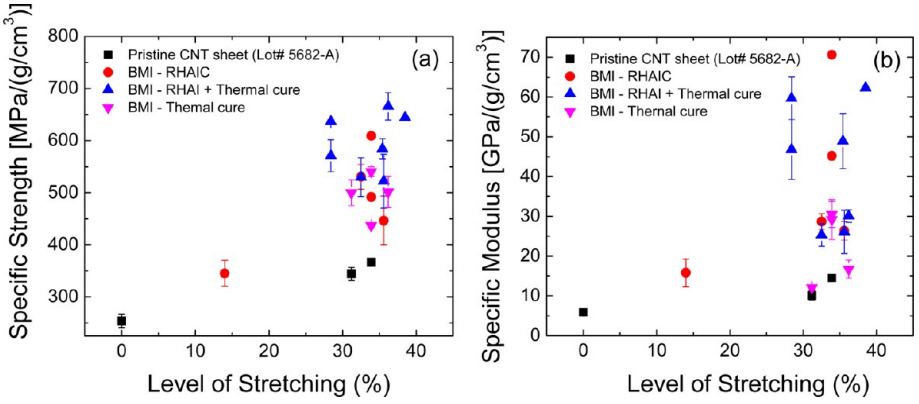

Figure 7. Comparison of (a) the specific strength and (b) specific modulus of pristine and stretched CNT sheets and processed BMI/CNT sheet nanocomposites in terms of the level of stretching. The BMI/CNT sheet nanocomposites were fabricated by thermal cure, RHAIC, and RHAI followed by post-thermal cure. The starting pristine CNT sheet was acetone treated from Lot# 5682-A.

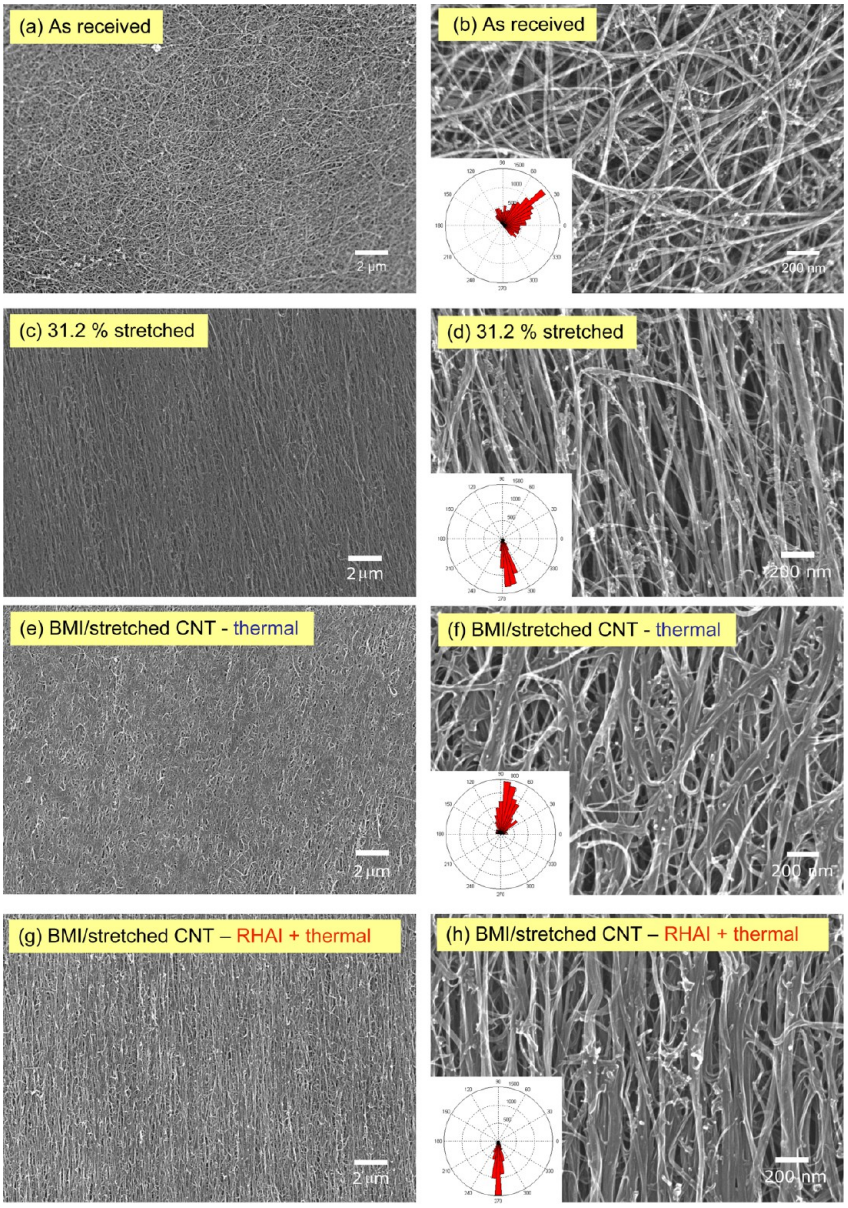

Figure 8. FE-SEM images of (a and b) as-received, (c and d) 31.2% stretched pristine CNT sheets, and BMI/stretched CNT sheet nanocomposites cured by (e and f) thermal and (g and h) RHAI followed by post-thermal cure. Inset: rose plots of the histogram of angular orientation obtained from each FE-SEM image.

from the relatively unaligned as-received sheet (Figure 8b) to the stretched sheet (Figure 8d) is reflected in the increase of the order parameter from $S = 0.240$ to $S = 0.796$. Also, note that the CNT sheet was significantly densified along the $x-y$ plane and thickened somewhat in the z-direction due to the auxetic behavior of CNT sheet during the stretching.[35] Adding BMI to the stretched sheet without RHAI and curing in an oven results in the structure shown in Figure 8f. Relaxing tension prior to curing the material clearly results in the loss of some orientation, which is confirmed by a reduction of the order parameter to $S = 0.541$. If, instead, the tension is maintained and the CNT sheet is infiltrated and partially cured using RHAI, much of the orientation is maintained and the order parameter is found to be $S = 0.789$.

To investigate the extent of BMI resin cure achieved with the resistive heating method, FTIR and DSC experiments were conducted on several nanocomposite samples. The specimens were fabricated by stretching CNT sheets by 40%, infiltrating with the BMI solution, and drying. The FTIR spectrum of the uncured BMI/CNT sample (Figure 9a) exhibited strong absorption bands around 1709 (imide carbonyl), 1511 (phenyl ring), 1393 (imide ring), and 833 cm^{-1} (phenyl and maleimide ring). After thermally curing the sample for 6 h at 240 °C, these absorption bands were still evident, albeit at reduced intensities (Figure 9a). For another sample cured by RHAIC (10 V, 7 A for 30 min), small absorptions are apparent around 1709, 1511, and 1393 cm^{-1}, but much less intense than those from the thermal cure. In addition, the fingerprint region (1000−500 cm^{-1}) is devoid of any peaks, indicating complete cure of the BMI resin.[50] The spectra for both the specimen processed by RHAI followed by thermal cure (240 °C, 6 h) and the sample prepared by press molding are nearly identical to that of the RHAIC processed specimen. The FTIR results indicate that the specimens treated by RHAIC have achieved a complete degree

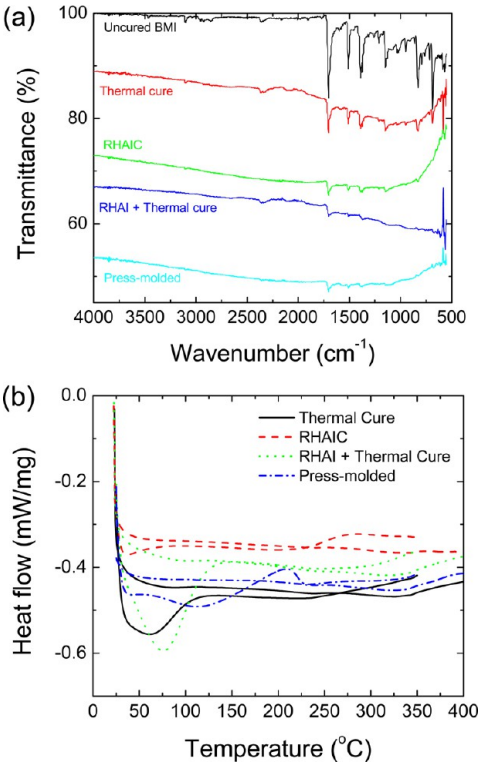

Figure 9. (a) FTIR spectra of uncured BMI/CNT and as-prepared BMI/CNT sheet nanocomposites via thermal cure, RHAIC, RHAI followed by thermal cure, and press-molded cure. (b) DSC thermographs of as-prepared BMI/CNT sheet nanocomposites via thermal cure, RHAIC, RHAI followed by thermal cure, and press-molded cure.

of cure in a significantly reduced time period compared to thermal cure.

The same BMI/CNT specimens were also characterized by DSC. The samples were heated to 350 °C, quench cooled and subsequently heated to 400 °C (Figure 9b). Except for the press-molded sample, none of the samples showed significant transitions, instead exhibiting only minor changes in the baseline at around 250 to 300 °C. On the first run of the press-molded sample, an exothermic peak centered near 220 °C was apparent, but disappeared on the second run. No glass transitions (Tg) were apparent in any of the samples, which is not uncommon in thermosetting CFRPs. The DSC results support the FTIR data indicating that the RHAIC process cures the BMI to an extent equal to or greater than the other cure methods investigated.

Demonstrating the effectiveness of the RHAI processing method for a single layer CNT sheet is an important proof of concept, but any practical application will require the fabrication of much thicker composites. As a first step in this direction, BMI/CNT sheet nanocomposites were prepared with two layers of CNT sheets by RHAI followed by thermal cure, both with and without press-molding. Two layers of CNT sheet were overlaid and then stretched to the desired degree. The orientation of the stretching between each sheet is presumably 0°. One set of the stretched CNT sheets was then processed by RHAI followed by thermal cure as described above for the single sheets. A second set of stretched and BMI infiltrated CNT sheet was clamped, transferred to the mold under tension, and then postcured under high pressure (500 psi, 3.44 MPa). The resulting mechanical data are summarized in Table 2 and Figure 10. In view of the different degrees of stretching that were achieved in the various samples and the error bars associated with their values, it is difficult to draw any strong conclusions from these results. It is, however, encouraging that adding a second layer did not measurably reduced the specific mechanical properties relative to single sheet composites. This indicates that the two layer composites did not have significant resin rich layers, which can promote failure by interlayer delamination or sliding between the two CNT sheets. This inference is supported by the SEM images shown in Figure 11e,f.

Pristine CNT sheets have been shown to fail in various ways, including breaking, sliding, debundling, telescoping, and delamination.[35,51] With the addition of BMI resin, the partially failed BMI-coated CNTs (Figure 11b) were pulled from the CNT bundles under a continuous tensile load. Partially broken CNTs and CNT bundles, which had cleaner and thinner surfaces, bridged the cracks (Figure 11c,d) until complete failure of the material occurred. The mechanical properties of the nanocomposites could potentially be further enhanced by chemical functionalization of CNT surfaces to provide covalent bonding between the infiltrated resin and CNT[52−54] or by inter/intratube bonding of CNTs by electron beam irradiation.[55−59] Additional studies are underway to examine the potential of resistive heating assisted nanocomposite fabrication to further enhance the mechanical properties of CNT sheet nanocomposites using purified (catalyst removed) and/or chemically functionalized CNT sheets.

Table 2. Physical and Mechanical Properties of Pristine and Processed BMI/CNT Sheet Nanocomposites

sample	cure	stretching level (%)	density (g/cm^3)	thickness (μm)	specific strength [MPa/(g/cm^3)]	specific modulus [GPa/(g/cm^3)]	elongation at failure (%)
pristine (Lot# 70044)		0	0.709	17.4	253 ± 4	5.8 ± 0.6	40 ± 1
BMI/CNT sheet (1 ply)	thermal	0	0.756	23.5	357 ± 14	21 ± 2	16 ± 1
BMI/S-CNT sheet (1 ply)	RHAI + thermal	41	0.662	38.7	549 ± 22	49 ± 11	2.7 ± 1.0
BMI/S-CNT sheet (2 ply)	RHAI + thermal	33	1.004	40.6	467 ± 39	40 ± 3	2.0 ± 0.2
BMI/S-CNT sheet (2 ply)	RHAI + thermal	36	0.663	57.9	509 ± 38	35 ± 3	4.2 ± 1.2
BMI/S-CNT sheet (1 ply)	RHAI + press-mold	48	0.701	40.2	578 ± 64	41 ± 7	2.5 ± 0.2
BMI/S-CNT sheet (2 ply)	RHAI + press-mold	42	0.749	74.4	602 ± 30	52 ± 3	2.1 ± 0.5

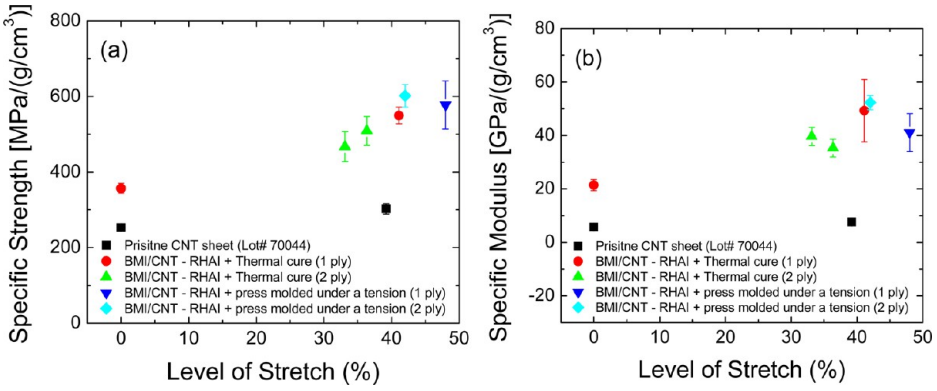

Figure 10. Comparison of (a) the specific strength and (b) specific modulus of pristine and processed BMI/CNT sheet nanocomposites in terms of the level of stretching. The BMI/CNT sheet nanocomposites were fabricated by RHAI followed by post-thermal cure or press-mold. The starting acetone treated CNT sheet was from Lot# 70044.

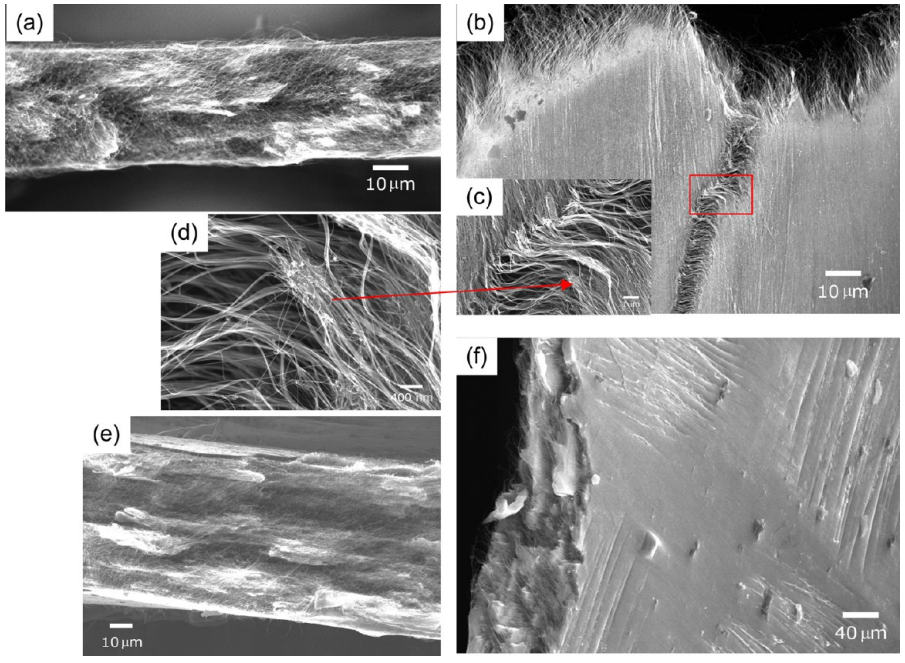

Figure 11. FE-SEM images of BMI/CNT sheet (1 ply and 36% stretched) nanocomposites fabricated by RHAI followed by thermal cure. (a) Cross-sectional and (b, c, and d) top surface after tensile failure. The BMI/CNT sheet nanocomposite processed by RHAI followed by press-mold cure was fabricated with two layers of CNT sheet (42% stretching) and its (e) cross-sectional and (f) tilted FE-SEM images were taken at the failure site.

4. CONCLUSION

Various nanocomposite fabrication processes intended to enhance the mechanical properties of CNT sheet nanocomposites for structural applications were investigated and demonstrated. These included mechanical stretching, thermal curing, resin infiltration and curing by resistive heating, and combinations thereof. The CNTs and CNT bundles were aligned and densified by mechanical stretching. CNT alignment was effectively locked in with polymer resin by employing a resistive heating process to achieve rapid and efficient resin wetting and cure. This process was shown to improve load transfer through prevention of shear sliding between the tubes, as well as between the CNT layers. By using the resistive heating process, the time to fully cure thermosetting resins can be significantly reduced. This fabrication method is not limited to thermoset matrixes, but can be applied to other classes of polymers where an increase in resin temperature yields lower viscosity. Although the example studied used CNT sheet reinforcement, this method can be applied to other reinforcements such as highly densified CNT yarns or fuzzy carbon fibers.

AUTHOR INFORMATION

Corresponding Authors

*J.-W.K. E-mail: jae-woo.kim-1@nasa.gov.
*E.J.S. E-mail: emilie.j.siochi@nasa.gov.

Notes

The authors declare no competing financial interest.

ACKNOWLEDGMENTS

This work was funded through the NASA Game Changing Development Program/Nanotechnology Project.

REFERENCES

(1) Treacy, M. M. J.; Ebbesen, T. W.; Gibson, J. M. Exceptionally High Young's Modulus Observed for Individual Carbon Nanotubes. *Nature* **1996**, *381*, 678−680.

(2) Wong, E. W.; Sheenhan, P. E.; Lieber, C. M. Nanobeam Mechanics: Elasticity, Strength, and Toughness of Nanorods and Nanotubes. *Science* **1997**, *277*, 1971−1975.

(3) Yu, M.-F.; Lourie, O.; Dyer, M. J.; Moloni, K.; Kelly, T. F.; Ruoff, R. S. Strength and Breaking Mechanism of Multiwalled Carbon Nanotubes Under Tensile Load. *Science* **2000**, *287*, 637−640.

(4) Zhu, Y.; Espinosa, H. D. An Electromechanical Material Testing System for in Situ Electron Microscopy and Applications. *Proc. Natl. Acad. Sci. U. S. A.* **2005**, *102*, 14503−14508.

(5) Xie, X.-L.; Mai, Y.-W.; Zhu, X.-P. Dispersion and Alignment of Carbon Nanotubes in Polymer Matrix: A Review. *Mater. Sci. Eng. R* **2005**, *49*, 89−112.

(6) Moniruzzaman, M.; Winey, K. I. Polymer Nanocomposites Containing Carbon Nanotubes. *Macromolecules* **2006**, *39*, 5194−5205.

(7) Coleman, J. N.; Khan, U.; Blau, W. J.; Gun'ko, Y. K. Small but Strong: A Review of the Mechanical Properties of Carbon Nanotube-Polymer Composites. *Carbon* **2006**, *44*, 1624−1652.

(8) Spitalsky, Z.; Tasis, D.; Papagelis, K.; Galiotis, C. Carbon Nanotube-Polymer Composites: Chemistry, Processing, Mechanical and Electrical Properties. *Prog. Polym. Sci.* **2010**, *35*, 357−401.

(9) Byrne, M. T.; Gun'ko, Y. K. Recent Advances in Research on Carbon Nanotube-Polymer Composites. *Adv. Mater.* **2010**, *22*, 1672−1688.

(10) Ajayan, P. M.; Schadler, L. S.; Giannaris, C.; Rubio, A. Single-Walled Carbon Nanotube-Polymer Composites: Strength and Weakness. *Adv. Mater.* **2000**, *12*, 750−753.

(11) Fiedler, B.; Gojny, F. H.; Wichmann, M. H. G.; Nolte, M. C. M.; Schulte, K. Fundamental Aspects of Nano-Reinforced Composites. *Compos. Sci. Technol.* **2006**, *66*, 3115−3125.

(12) Krishnamoorti, R. Strategies for Dispersing Nanoparticles in Polymers. *MRS Bull.* **2007**, *32*, 341−347.

(13) Kashiwagi, T.; Fagan, J.; Douglas, J. F.; Yamamoto, K.; Heckert, A. N.; Leigh, S. D.; Obrzut, J.; Du, F.; Lin-Gibson, S.; Mu, M.; Winey, K. I.; Haggenmueller, R. Relationship Between Dispersion Metric and Properties of PMMA/SWNT Nanocomposites. *Polymer* **2007**, *48*, 4855−4866.

(14) Baur, J.; Silverman, E. Challenges and Opportunities in Multifunctional Nanocomposite Structures for Aerospace Applications. *MRS Bull.* **2007**, *32*, 328−334.

(15) Sreekumar, T. V.; Liu, T.; Kumar, S.; Ericson, L. M.; Hauge, R. H.; Smalley, R. E. Single-Wall Carbon Nanotube Films. *Chem. Mater.* **2003**, *15*, 175−178.

(16) Ma, W.; Song, L.; Yang, R.; Zhang, T.; Zhao, Y.; Sun, L.; Ren, Y.; Liu, D.; Liu, L.; Shen, J.; Zhang, Z.; Xiang, Y.; Zhou, W.; Xie, S. Directly Synthesized Strong, Highly Conducting, Transparent Single-Walled Carbon Nanotube Films. *Nano Lett.* **2007**, *7*, 2307−2311.

(17) Chen, I.-W. P.; Liang, R.; Zhao, H.; Wang, B.; Zhang, C. Highly Conductive Carbon Nanotube Buckypapers with Improved Doping Stability via Conjugational Cross-Linking. *Nanotechnology* **2011**, *22*, 485708.

(18) Zhu, H. W.; Xu, C. L.; Wu, D. H.; Wei, B. Q.; Vajtai, R.; Ajayan, P. M. Direct Synthesis of Long Single-Walled Carbon Nanotube Strands. *Science* **2002**, *296*, 884−886.

(19) Ericson, L. M.; Fan, H.; Peng, H.; Davis, V. A.; Zhou, W.; Sulpizio, J.; Wang, Y.; Booker, R.; Vavro, J.; Guthy, C.; Parra-Vasquez, A. N. G.; Kim, M. J.; Ramesh, S.; Saini, R. K.; Kittrell, C.; Lavin, G.; Schmidt, H.; Adams, W. W.; Billups, W. E.; Pasquali, M.; Hwang, W.-F.; Hauge, R. H.; Fischer, J. E.; Smalley, R. E. Macroscopic, Neat, Single-Walled Carbon Nanotube Fibers. *Science* **2004**, *305*, 1447−1450.

(20) Zhang, M.; Atkinson, K. R.; Baughman, R. H. Multifunctional Carbon Nanotube Yarns by Downsizing an Ancient Technology. *Science* **2004**, *306*, 1358−1361.

(21) Zhang, Z.; Jiang, K.; Feng, C.; Liu, P.; Zhang, L.; Kong, J.; Zhang, T.; Li, Q.; Fan, S. Spinning and Processing Continuous Yarns from 4-Inch Wafer Scale Super-Aligned Carbon Nanotube Arrays. *Adv. Mater.* **2006**, *18*, 1505−1510.

(22) Koziol, K.; Vilatela, J.; Moisala, A.; Motta, M.; Cunniff, P.; Sennett, M.; Windle, A. High-Performance Carbon Nanotube Fiber. *Science* **2007**, *318*, 1892−1895.

(23) Lu, W.; Zu, M.; Byun, J.-H.; Kim, B.-S.; Chou, T.-W. State of the Art of Carbon Nanotube Fibers: Opportunities and Challenges. *Adv. Mater.* **2012**, *24*, 1805−1833.

(24) Behabtu, N.; Young, C. C.; Tsentalovich, D. E.; Kleinerman, O.; Wang, X.; Ma, A. W. K.; Amram Bengio, E.; ter Waarbeek, R. F.; de Jong, J. J.; Hoogerwerf, R. E.; Fairchild, S. B.; Ferguson, J. B.; Maruyama, B.; Kono, J.; Talmon, Y.; Cohen, Y.; Otto, M. J.; Pasquali, M. Strong, Light, Multifunctional Fibers of Carbon Nanotubes with Ultrahigh Conductivity. *Science* **2013**, *339*, 182−186.

(25) Wang, Z.; Liang, Z.; Wang, B.; Zhang, C.; Kramer, L. Processing and Property Investigation of Single-Walled Carbon Nanotube (SWNT) Buckypaper/Epoxy Resin Matrix Nanocomposites. *Composites, Part A* **2004**, *35*, 1225−1232.

(26) Ma, W.; Liu, L.; Zhang, Z.; Yang, R.; Liu, G.; Zhang, T.; An, X.; Yi, X.; Ren, Y.; Niu, Z.; Li, J.; Dong, H.; Zhou, W.; Ajayan, P. M.; Xie, S. High-Strength Composite Fibers: Realizing True Potential of Carbon Nanotubes in Polymer Matrix Through Continuous Reticulate Architecture and Molecular Level Couplings. *Nano Lett.* **2009**, *9*, 2855−2861.

(27) Cheng, Q. F.; Wang, J. P.; Wen, J. J.; Liu, C. H.; Jiang, K. L.; Li, Q. Q.; Fan, S. S. Carbon Nanotube/Epoxy Composites Fabricated by Resin Transfer Molding. *Carbon* **2010**, *48*, 260−266.

(28) Cheng, Q.; Wang, B.; Zhang, C.; Liang, Z. Functionalized Carbon-Nanotube Sheet/Bismaleimide Nanocomposites: Mechanical and Electrical Performance Beyond Carbon-Fiber Composites. *Small* **2010**, *6*, 763−767.

(29) Cheng, Q.; Bao, J.; Park, J. G.; Liang, Z.; Zhang, C.; Wang, B. High Mechanical Performance Composite Conductor: Multi-Walled Carbon Nanotube Sheet/Bismaleimide Nanocomposites. *Adv. Funct. Mater.* **2009**, *19*, 3219−3225.

(30) Dalton, A. B.; Muñoz, E.; Collins, S.; Kim, B. G.; Razal, J.; Selvidge, M.; Vieiro, G.; Baughman, R. H. Improving the Mechanical Properties of Single-Walled Carbon Nanotube Sheets by Intercalation of Polymeric Adhesives. *Appl. Phys. Lett.* **2003**, *82*, 1682−1684.

(31) Xu, G.; Zhang, Q.; Zhou, W.; Huang, J.; Wei, F. The Feasibility of Producing MWCNT Paper and Strong MWCNT Film from VACNT Array. *Appl. Phys. A: Mater. Sci. Process.* **2008**, *92*, 531−539.

(32) Shim, B. S.; Zhu, J.; Jan, E.; Critchley, K.; Ho, S.; Podsiadlo, P.; Sun, K.; Kotov, N. A. Multiparameter Structural Optimization of Single-Walled Carbon Nanotube Composites: Toward Record Strength, Stiffness, and Toughness. *ACS Nano* **2009**, *3*, 1711−1722.

(33) Li, Y.; Kröger, M. A Theoretical Evaluation of the Effects of Carbon Nanotube Entanglement and Bundling on the Structural and Mechanical Properties of Buckypaper. *Carbon* **2012**, *50*, 1793−1806.

(34) Wang, S.; Haldane, D.; Liang, R.; Smithyman, J.; Zhang, C.; Wang, B. Nanoscale Infiltration Behaviour and Through-Thickness Permeability of Carbon Nanotube Buckypapers. *Nanotechnology* **2013**, *24*, 015704.

(35) Kim, J.-W.; Siochi, E. J.; Carpena-Núñez, J.; Wise, K. E.; Connell, J. W.; Lin, Y.; Wincheski, R. A. Polyaniline/Carbon Nanotube Sheet Nanocomposites: Fabrication and Characterization. *ACS Appl. Mater. Interfaces* **2013**, *5*, 8597−8606.

(36) Liu, W.; Zhang, X.; Xu, G.; Bradford, P. D.; Wang, X.; Zhao, H.; Zhang, Y.; Jia, Q.; Yuan, F.-G.; Li, Q.; Qiu, Y.; Zhu, Y. Producing Superior Composites by Winding Carbon Nanotubes onto a Mandrel under a Poly(vinyl alcohol) Spray. *Carbon* **2011**, *49*, 4786−4791.

(37) Di, J.; Hu, D.; Chen, H.; Yong, Z.; Chen, M.; Feng, Z.; Zhu, Y.; Li, Q. Ultrastrong, Foldable, and Highly Conductive Carbon Nanotube Film. *ACS Nano* **2012**, *6*, 5457−5464.

(38) Liu, Y.-N.; Li, M.; Gu, Y.; Wang, K.; Hu, D.; Li, Q.; Zhang, Z. A Modified Spray-Winding Approach to Enhance the Tensile Performance of Array-Based Carbon Nanotube Composite Films. *Carbon* **2013**, *65*, 187−195.

(39) Lee, W. I.; Springer, G. S. Microwave Curing of Composites. *J. Compos. Mater.* **1984**, *18*, 387−409.
(40) Hoogenboom, R.; Schubert, U. S. Microwave-Assisted Polymer Synthesis: Recent Developments in a Rapidly Expanding Field of Research. *Macromol. Rapid Commun.* **2007**, *28*, 368−386.
(41) Kumar, P. K.; Raghavendra, N. V.; Sridhara, B. K. Development of Infrared Radiation Curing System for Fiber Reinforced Polymer Composites: An Experimental Investigation. *Indian J. Eng. Mater. Sci.* **2011**, *18*, 24−30.
(42) Levy, A.; Le Corre, S.; Poitou, A. Ultrasonic Welding of Thermoplastic Composites: A Numerical Analysis at the Mesoscopic Scale Relating Processing Parameters, Flow of Polymer and Quality of Adhesion. *Int. J. Mater. Form.* **2014**, *7*, 39−51.
(43) Bayerl, T.; Duhovic, M.; Mitschang, P.; Bhattacharyya, D. The Heating of Polymer Composites by Electromagnetic Induction − A Review. *Composites, Part A* **2014**, *57*, 27−40.
(44) Meng, F.; Zhang, X.; Li, R.; Zhao, J.; Xuan, X.; Wang, X.; Zou, J.; Li, Q. Electro-Induced Mechanical and Thermal Responses of Carbon Nanotube Fibers. *Adv. Mater.* **2014**, *26*, 2480−2485.
(45) Sundaresan, V. B.; Morgan, A.; Castellucci, M. Self-Healing of Ionomeric Polymers with Carbon Fibers from Medium-Velocity Impact and Resistive Heating. *Smart Mater. Res.* **2013**, *2013*, Article ID: 271546.
(46) Pierson, H. O. *Handbook of Carbon, Graphite, Diamond and Fullerenes: Properties, Processing and Applications*; Noyes Publications, Park Ridge, NJ, 1993.
(47) Zamora-Ledezma, C.; Blanc, C.; Maugey, M.; Zakri, C.; Poulin, P.; Anglaret, E. Anisotropic Thin Films of Single-Wall Carbon Nanotubes from Aligned Lyotropic Nematic Suspension. *Nano Lett.* **2008**, *8*, 4103−4107.
(48) Wulf, M.; Uhlmann, P.; Michel, S.; Grundke, K. Surface Tension Studies of Levelling Additives in Powder Coatings. *Prog. Org. Coat.* **2000**, *38*, 59−66.
(49) Liu, T.; Kumar, S. Effect of Orientation on the Modulus of SWNT Films and Fibers. *Nano Lett.* **2003**, *3*, 647−650.
(50) Satheesh Chandran, M.; Krishna, M.; Salini, K.; Rai, K. S. Preparation and Characterization of Chain-Extended Bismaleimide/Carbon Fibre Composites. *Int. J. Polym. Sci.*, **2010**, *2010*, Article ID: 987357.
(51) Yu, M.-F.; Yakobson, B. I.; Ruoff, R. S. Controlled Sliding and Pullout of Nested Shells in Individual Multiwalled Carbon Nanotubes. *J. Phys. Chem. B* **2000**, *104*, 8764−8767.
(52) Sun, Y.-P.; Fu, K.; Lin, Y.; Huang, W. Functionalized Carbon Nanotubes: Properties and Applications. *Acc. Chem. Res.* **2002**, *35*, 1096−1104.
(53) Tasis, D.; Tagmatarchis, N.; Bianco, A.; Prato, M. Chemistry of Carbon Nanotubes. *Chem. Rev.* **2006**, *106*, 1105−1136.
(54) Sahoo, N. G.; Rana, S.; Cho, J. W.; Li, L.; Chan, S. H. Polymer Nanocomposites Based on Functionalized Carbon Nanotubes. *Prog. Polym. Sci.* **2010**, *35*, 837−867.
(55) Kris, A.; Csanyi, G.; Salvetat, J.-P.; Lee, T.-N.; Couteau, E.; Kulik, A. J.; Beniot, W.; Brugger, J.; Forro, L. Reinforcement of Single-Walled Carbon Nanotube Bundles by Intertube Bridging. *Nat. Mater.* **2004**, *3*, 153−157.
(56) Krasheninnikov, A. V.; Banhart, F. Engineering of Nanostructured Carbon Materials with Electron or Ion Beams. *Nat. Mater.* **2007**, *6*, 723−733.
(57) Peng, B.; Locascio, M.; Zapol, P.; Li, S.; Mielke, S.; Schatz, G. C.; Espinosa, H. D. Measurements of Near-Ultimate Strength for Multiwalled Carbon Nanotubes and Irradiation-Induced Cross-Linking Improvements. *Nat. Nanotechnol.* **2008**, *3*, 626−631.
(58) Filleter, T.; Bernal, R.; Li, S.; Espinosa, H. D. Ultrahigh Strength and Stiffness in Cross-Linked Hierarchical Carbon Nanotube Bundles. *Adv. Mater.* **2011**, *23*, 2855−2860.
(59) Filleter, T.; Espinosa, H. D. Multi-Scale Mechanical Improvement Produced in Carbon Nanotube Fibers by Irradiation Cross-Linking. *Carbon* **2013**, *56*, 1−11.